JOURNAL OF MATERIALS SCIENCE 27 (1992) 4501–4510

Observations on the crack-enhanced creep–fracture of a polycrystalline alumina with a glassy grain-boundary phase

K. Y. DONALDSON, A. VENKATESWARAN, D. P. H. HASSELMAN
Department of Materials Engineering, Virginia Polytechnic Institute and State University, Blacksburg, VA 24061, USA

An experimental study was conducted of the role of cracks in the creep–rupture behaviour of a polycrystalline alumina with glassy grain-boundary phase at stress regimes and temperatures at which failure is anticipated to occur from pre-existing flaws. Samples were tested without and with artificial flaws in the form of slots or indentation cracks. All three sample types exhibited non-linear creep. The relative rate of increase in creep rate with increasing dimension of slot-depth greatly exceeded the corresponding increase in specimen compliance, as expected for non-linear creep. An analysis of the data indicated that the observed creep behaviour was primarily controlled by crack-enhanced creep with a minor contribution from elastic creep by crack growth. Very poor correlations were found for the stress dependence of the creep rate and time-to-failure. In terms of Monkman–Grant behaviour, good correlations existed between creep rate and time-to-failure, independent of stress and size of the slots or indentation cracks. Because failure originated from pre-existing flaws, the experimental findings of this study suggest the existence of a failure mechanism referred to by the present authors as "crack-enhanced creep fracture".

1. Introduction

The successful utilization of structural ceramics in high-temperature applications will critically depend on their stress–rupture behaviour, i.e. their time-to-failure under load, at temperatures sufficiently high that creep deformation occurs concurrently with the development and growth of cracks responsible for the time-dependent fracture. A number of recent studies have focused on the basic mechanisms which underlie the creep–rupture of structural ceramics, including the propagation of pre-existing cracks, the nucleation of new cracks, the development of the damage (i.e. the microcracks) which accompanies macro-crack growth and the role of any glassy phase present at the grain boundaries [1–9].

The specific mechanism of failure due to creep–rupture appears to be a function of the stress level [3]. At high stresses, failure is controlled by the growth of pre-existing cracks. The stress dependence of the failure time is governed by the dependence of the rate of crack growth on the stress intensity factor. Quinn [6] observed that, for a polycrystalline aluminium oxide, the measured value of the exponent for the dependence of crack velocity on stress intensity factor agreed very well with the value inferred from the dependence of time-to-failure on applied stress in creep–rupture. This suggests that at least for the experimental conditions selected by Quinn, the time-to-failure was controlled by the growth of pre-existing cracks. In terms of the findings of the present study, it should be noted that the data of Quinn showed a very large scatter in the times-to-failure at any given stress level. This is also expected for failure from pre-existing cracks, in direct analogy to the large scatter in failure times observed for the static fatigue of brittle materials at ambient temperatures under environmental conditions where crack growth is controlled by mechanisms of stress corrosion. It should be noted also that for stress–rupture controlled by the growth of pre-existing cracks, a direct inverse relationship between time-to-failure and creep rates is not expected. For instance, the data of Wiederhorn *et al.* [5] for an alumina with a glassy grain-boundary phase show an excellent correlation between creep rate and stress at a given temperature, whereas the corresponding data for the time-to-failure as a function of stress show a much greater degree of scatter. In the view of these authors this suggests that in the experiments of Wiederhorn *et al.* [5], creep deformation and the time-to-failure are governed by different independent mechanisms. Clearly, because both creep and the rate of growth of pre-existing cracks at high-temperature are governed by stress-dependent thermally activated processes, general correlations are to be expected between data for creep rate and time-to-failure, but no direct correlation is expected from specimen to specimen.

At lower stress levels, failure occurs from the nucleation and the creep-constrained growth of cracks [3].

0022–2461

In this case the stress dependence of the time-to-failure will be governed by the stress dependence of the creep deformation. Creep rate and time-to-failure will exhibit the typical Monkman–Grant [10] type of relationship. The rate of creep deformation for specimens of the same batch are expected to show good correlation with the magnitude of stress. For this reason, because crack growth is creep controlled, times-to-failure are also expected to show good correlations with stress and are not expected to exhibit the extensive data scatter observed for failure by the growth of pre-existing flaws. Indeed, for a fine-grained polycrystalline alumina (AlSiMag 838, General Electric Company) used in an earlier study for the effect of multiple crack growth on strain-rate sensitivity, the present authors [11] found correlation coefficients of 0.87 and 0.88 for the dependence of creep rate and time-to-failure on stress, respectively. The corresponding correlation for the relationship between creep rate and time-to-failure was also quite good, with a correlation coefficient of 0.87, which strongly suggests that the rate of growth of the failure-initiating crack was controlled by the accompanying creep process. More recently, however, similar measurements were made on another relatively coarse-grained polycrystalline aluminium oxide with a glassy grain-boundary phase, subjected to stress levels which were a substantial fraction of the short-term fracture stress at which failure would be expected to occur from the growth of pre-existing flaws. Very poor correlations were found for the stress dependence of the creep rate and time-to-failure, yet good correlation existed between creep rate and time-to-failure. Poor correlation between time-to-failure and stress is expected for samples with a wide variation in the size of the pre-existing flaws. However, failure from pre-existing flaws can occur from diffusional or other processes at the crack tip and does not require the existence of a creep process. For this reason the excellent correlation between creep rate and the time-to-failure, at least at first sight, appeared somewhat surprising. However, such correlations can be reconciled if the failure-originating cracks by some mechanism(s) contributed to or took an active part in the creep process itself. One such mechanism is crack-enhanced creep, originally suggested by Weertman [12] and pursued further by two of the authors of this paper [13, 14]. A further mechanism by which cracks can contribute to the creep process is based on the effect of cracks on the effective elastic properties of a solid. The growth of cracks leads to an increase in time-dependent elastic strain under load. This mechanism of creep, referred to as elastic creep, was originally suggested by Venkateswaran and Hasselman [15], and formulated further by Suresh and Brockenbrough [16] and experimentally verified by the present authors [11, 17]. In order to investigate the possible contribution of cracks to the creep process, a study was conducted of the creep–rupture behaviour of the coarse-grained alumina ceramic with glassy phase referred to above, using samples with deliberately introduced precracks. It is the purpose of this paper to report these results.

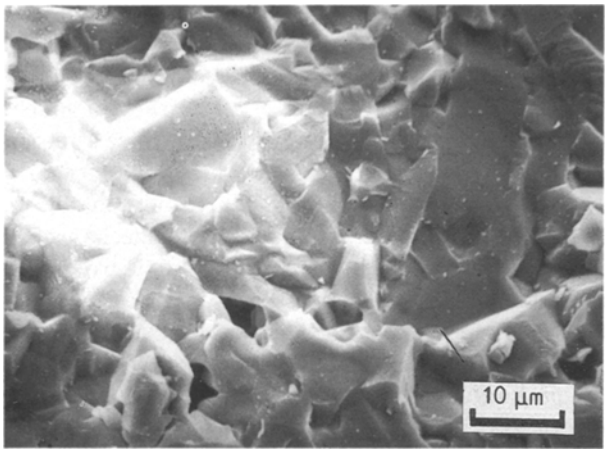

Figure 1 SEM fractograph of AD-94 alumina.

2. Experimental procedure

2.1. Materials

The polycrystalline alumina selected for this study consisted of AD-94 alumina (Coors Porcelain Company, Golden, CO), and was nominally identical to the alumina used in the study conducted by Quinn [6]. This alumina consists of nominally 94% alumina and a glassy grain-boundary phase with silicon, calcium, zirconium and magnesium as primary constituents. The scanning electron micrograph shown in Fig. 1 indicates that this alumina is nearly fully dense with grain sizes ranging from 1.5–13 μm and an average value of about 5–6 μm. Fig. 2 shows the distribution of magnesium, which represents an indication of the distribution of the glassy phase. It appears that the glassy phase is distributed in a highly heterogeneous fashion in the form of almost equi-dimensional inclusions contained within pockets of the alumina matrix phase and in the form of thin films along the grain boundaries.

The test samples for this alumina were in the form of as-fired circular rods about 50 mm in length with a diameter of ~ 6.25 mm. The samples were tested in the as-fired condition without additional surface treatment with the exception that prior to testing all samples were annealed at $\sim 825\,^{\circ}C$ for 6–7 h.

2.3. Test procedures

The specimens were tested in four-point bending with inner and outer spans of 10 and 40 mm, respectively. The specimen holder consisted of graphite, the load to the specimens being transferred by graphite pins which were permitted to rotate freely in order to keep extraneous stresses to a minimum. Testing was done in identical equipment to that used for earlier studies [11, 17] and consisted of an environmental chamber resistively heated with tungsten mesh heating elements in an argon atmosphere. The environmental chamber was contained within the load frame of an electro-hydraulic closed-loop mechanical tester. The displacement of the actuator and the resulting load were transferred via graphite push-rods and water-cooled

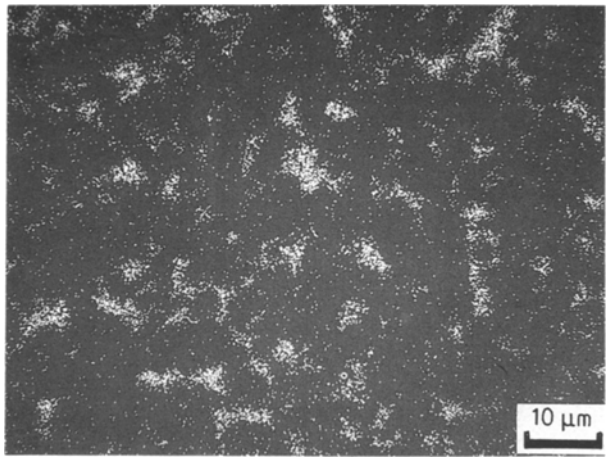

Figure 2 Distribution of magnesium within AD-94 alumina.

bellows to the specimen and load-cell, respectively. The displacement of the actuator during the period of mechanical loading was measured using a displacement gauge held against the actuator outside the environmental chamber. This gauge, with a range of approximately 4 mm, permitted measurements of the displacement to an accuracy of a few micrometres. By making a separate measurement of the elastic displacement of the total load train at the test temperature without the specimen, the displacement of the loading points of the specimens could be obtained by the appropriate subtraction. For the test specimens of this study the elastic displacement of the test specimens and the load train were about equal. The displacement as a function of time was recorded with an x–y recorder. The data for displacement at a given load were converted to stress and strain using the theory for bending of homogeneous beams. Creep rates were determined from the slope of the creep-strain versus time curves at the point in the curve corresponding to the secondary creep regime.

Governed by the results of preliminary experiments, appropriate loads and test temperatures were selected to result in times-to-failure of a few minutes to $\sim$ 1 h. In comparison to other literature studies on the stress–rupture behaviour of structural ceramics, these failure times place the results of this study in the high-stress regime, with failure times governed by the growth of pre-existing cracks.

Precracks were introduced in the specimens in two ways: one set was prepared by introducing slots of varying depth into the samples using a 15 cm diameter, 1 mm thick diamond blade; the other set of samples was pre-cracked by introducing indentation cracks using a Vickers hardness indentor with indentation loads ranging from 0–400 N. These pre-cracked specimens were subjected to creep deformation under conditions identical to those described above. Furthermore, their effective elastic behaviour (i.e. their compliance, defined as v/P where v is the relative displacement between the inner and outer loading points and P is the load) was measured at room temperature at a constant displacement rate of 0.5 mm min^{-1}. For both the measurement of creep and compliance the notched specimens were oriented such that the notch was in that section of the specimen subjected to tensile loading with the crack front perpendicular to the direction of the applied load. The indented samples were oriented such that the indentation was located on the line of maximum tensile stress on the specimen surface.

In order to determine possible changes in the effective Young's modulus due to the growth of cracks during creep, a number of specimens without pre-cracks were deformed to about 80%–90% of the failure strain at the temperature and load level of the creep tests. The effective Young's modulus of these specimens was then obtained at room temperature from load–displacement data obtained in four-point bending with the specimen orientation identical to that for the high-temperature tests.

The fracture toughness at the test temperature of 1225 °C was determined by first introducing cracks into the specimen surface at room temperature using the indentation method over a range of indentation loads, followed by measuring the failure load at 1225 at a displacement rate of 0.5 mm min^{-1}. The fracture toughness was then calculated from the failure load by the method of Chantikul *et al.* [18].

In order to estimate the initial size of the failure-initiating crack, the stress required for rapid fracture was determined at 1225 °C using a displacement rate of 0.5 mm min^{-1}.

Following deformation and/or fracture, the specimens were examined by scanning electron microscopy for evidence of crack formation and other microstructural changes.

3. Results, discussion and conclusions

Fig. 3 shows typical creep curves for a range of stress values. In general, the creep behaviour exhibits the expected primary, secondary and tertiary creep. The range of the secondary regime, however, appears to be a relatively small fraction of the total creep deformation. This suggests that rather than representing structure-invariant creep, the secondary regime for these data may actually consist in the merging of the primary and tertiary creep regimes. The creep data reported represent the minimum values of creep rate at the inflection point between the primary and tertiary regime.

Fig. 4a–c show the experimental results for the stress dependence of the creep rate and time-to-failure and the Monkman–Grant plot, respectively, for the alumina specimens of this study deformed at 1225 °C. The corresponding slopes of the least-squares straight line through the data were 2.4, -0.14 and -0.66, with correlation coefficients of 0.40, 0.54 and 0.89, respectively. Clearly, the stress exponent of 2.4 indicates that the creep is non-linear. No attempt will be made to pin-point the exact mechanism. It is expected that the glassy phase plays a primary role. As indicated by the results of Lange *et al.* [7], Hsich [8], Wiederhorn *et al.* [5] and Dryden *et al.* [9], creep deformation involving a glassy grain-boundary phase

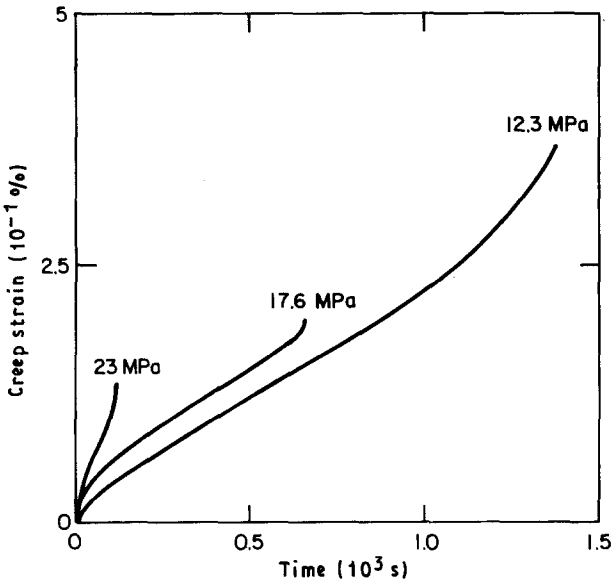

Figure 3 Typical creep curves for AD-94 alumina at 1225 °C for three different stress values.

is a function of its composition and degree of devitrification and whether the stress is tensile or compressive. Stress-dependent cavitation and crack growth contributing to stress-enhanced and elastic creep represent non-linear mechanisms of creep [13, 15, 16], may also have played a significant role. This mechanism also may have played a role in the present data because the value of strain for which the creep rate is reported already represents the onset of tertiary creep, due to the merging of the primary and tertiary creep regimes as discussed earlier.

The data for the stress dependence of the creep rate and time-to-failure presented in Fig. 4a and b show a great deal of scatter relative to the least-squares-fit straight line of the data and an almost order of magnitude variation in both creep rate and time-to-failure at any given value of stress. Such a degree of scatter in time-to-failure is not unexpected for fatigue failure under constant stress, controlled by crack-growth. But a corresponding scatter in creep data must be regarded as unusual. At first sight such scatter could be attributed to inconsistent experimental conditions. This effect, however, was not observed for other alumina materials investigated by these authors. Specimen-to-specimen variation should be considered as a distinct possibility, in particular, variation in the content of the glassy phase. At the high-stress regime of these studies, the failure time is expected to be governed by the growth of pre-existing cracks, rather than the nucleation and creep-constrained growth of new cracks. Even so, the creep rate and the time-to-failure are expected to exhibit correlations as both are expected to be affected by the viscous flow of the glassy grain-boundary phase. The growth of the failure-initiating flaw most likely will occur in glass-rich regions. The dimensions of such glass-rich regions, however, are expected to vary from specimen to specimen. Coupled with variation in the size of the failure-initiating flaw precursor, a large degree of scatter in

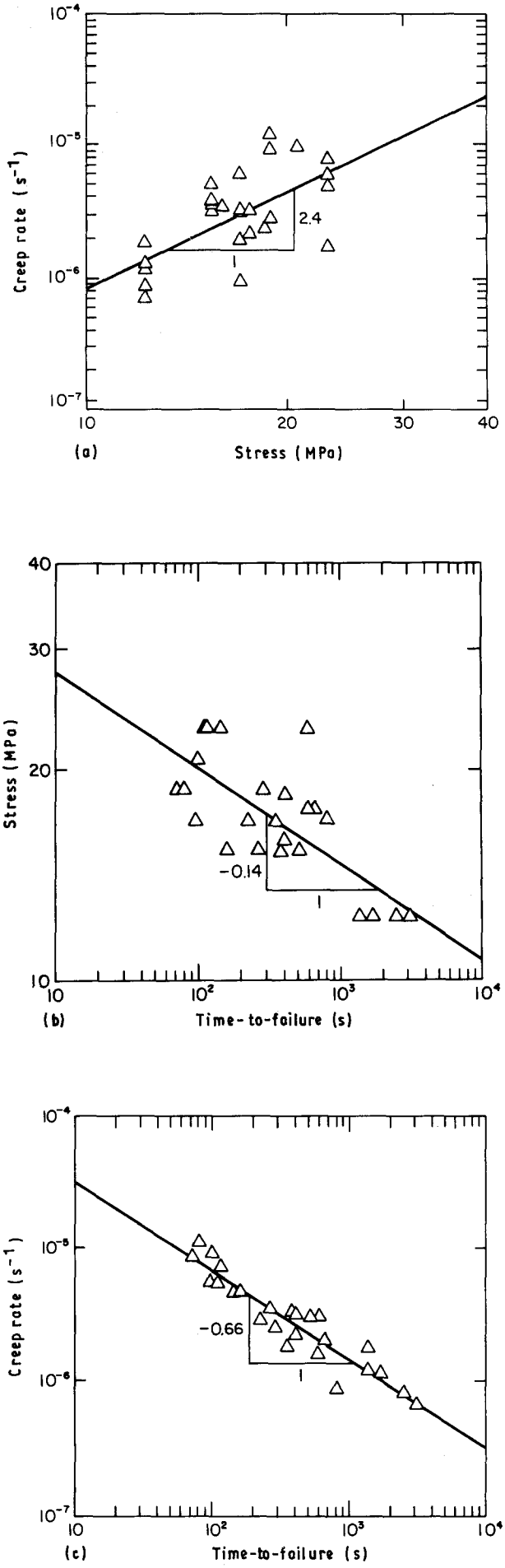

Figure 4 Experimental data for the creep–fracture behaviour of AD-94 alumina at 1225 °C: (a) stress dependence of creep rate; (b) stress dependence of time-to-failure; (c) Monkman–Grant plot of creep rate and time-to-failure.

times-to-failure is expected, as indicated by the experimental data. Creep deformation, however, is a function of the glass content of the specimen as a whole. Specimen-to-specimen variation in glass content is expected to be smaller than the variation in the local concentration of the glass content within any one specimen. For this reason, the degree of data scatter in the rate of creep deformation is expected to be smaller than the corresponding scatter in times-to-failure. This is not borne out by the experimental data for this alumina. In fact, the much higher correlation for the Monkman–Grant plot presented in Fig. 4c suggests a direct inverse relationship between creep rate and time-to-failure for any given specimen. As perceived by these authors, such a correlation suggests that the failure-initiating crack itself plays a role in the creep process. For this reason it is appropriate to examine the experimental results for the creep behaviour of samples with slots or indentation cracks.

Fig. 5a–c show the creep rate, time-to-failure and the Monkman–Grant behaviour for the slotted samples tested over a range of slot sizes at 1225 °C. The data presented in Fig. 5 indicate that the creep rate rises very rapidly with increasing slot depth. Even at values of slot depth small compared to the specimen diameter, the creep rate is significantly higher than for the non-slotted specimens. It should be pointed out also that these slotted samples also exhibit the typical primary, secondary and tertiary creep behaviour observed for the non-slotted samples shown in Fig. 4. The increase in creep rate due to the presence of the slot must be attributed primarily to the high stress concentration in the immediate vicinity of the notch. This, coupled with the non-linear nature of the creep process, leads to a large increase in creep rate. In general, the data in Fig. 5 represent experimental proof for the concept of crack-enhanced creep [12, 13]. As expected, the time-to-failure, as shown in Fig. 5b, decreases with increasing slot depth. It is interesting to note that the scatter in data for the rate of creep and the time-to-failure as a function of crack depth reflect the similar scatter in the data observed for the unslotted specimens presented in Fig. 4a and b. This scatter must be reflective of the heterogeneous nature of the material of this study and of compositional variation from specimen-to-specimen. Of particular interest is that this scatter in data is significantly reduced once the data are presented on the Monkman–Grant plot of Fig. 5c. Again, a one-to-one correspondence between the creep rate and the time-to-failure for any given specimen is strongly indicated, which lends credibility to the hypothesis that the rate of creep is affected by the presence of the crack.

The data for the specimens with the indentation cracks as a function of indentation load are similar to those obtained for the slotted samples, as shown by the data presented in Fig. 6a–c, for the creep rate, time-to-failure and Monkman–Grant behaviour. Fig. 7 shows the experimental data for the independently determined radius of the surface crack measured from a flat polished surface. Again, the creep rate and time-to-failure show a degree of scatter similar to the scatter observed for the as-received and slotted

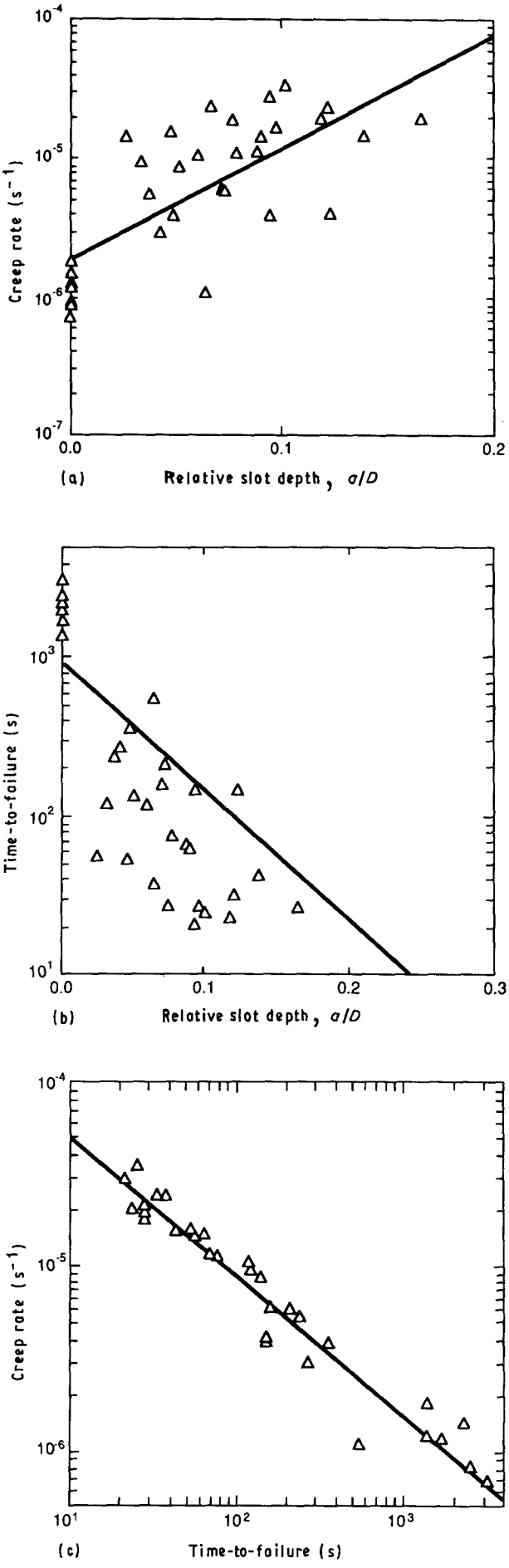

Figure 5 Experimental data for the creep–fracture behaviour of slotted samples of AD-94 alumina at 1225 °C and outer fibre stress of 12.3 MPa as a function of ratio of slot depth to specimen diameter: (a) creep rate; (b) time-to-failure; (c) Monkman–Grant plot.

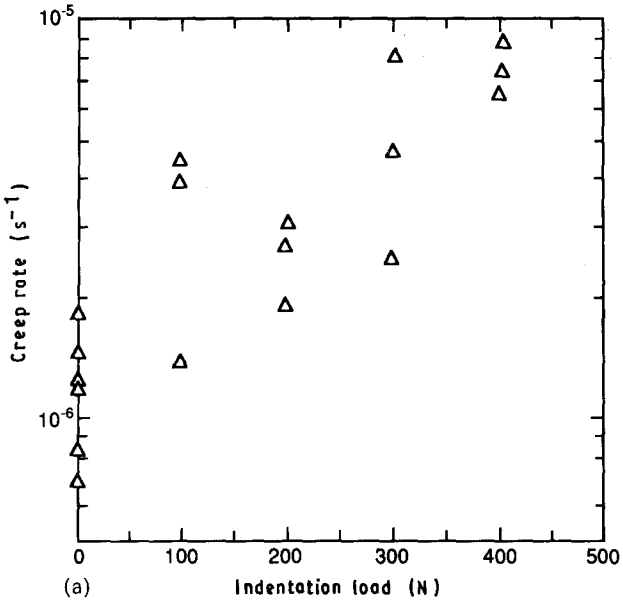

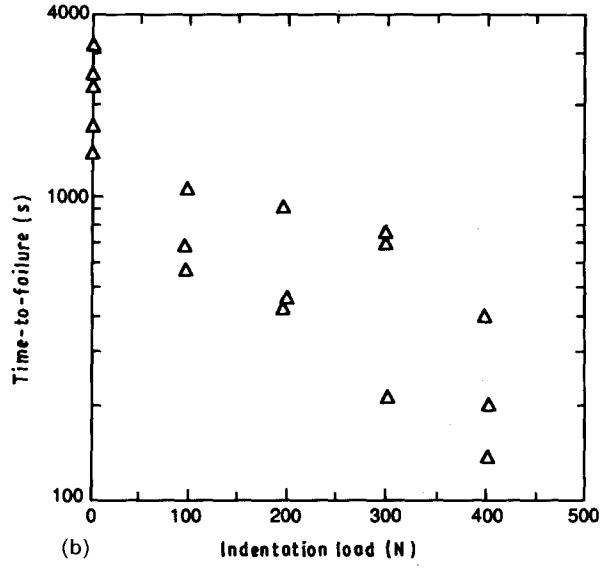

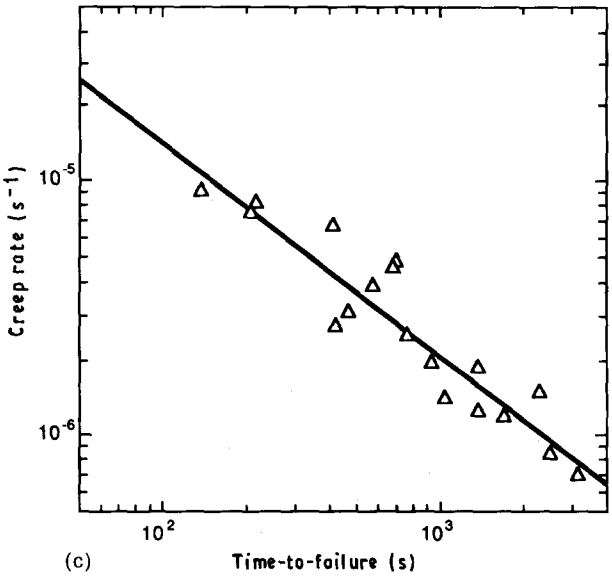

Figure 6 Experimental data for the creep–fracture behaviour of indented samples of AD-94 alumina at 1225 °C and outer fibre stress of 12.3 MPa as a function of indentation load: (a) creep rate; (b) time-to-failure; (c) Monkman–Grant plot.

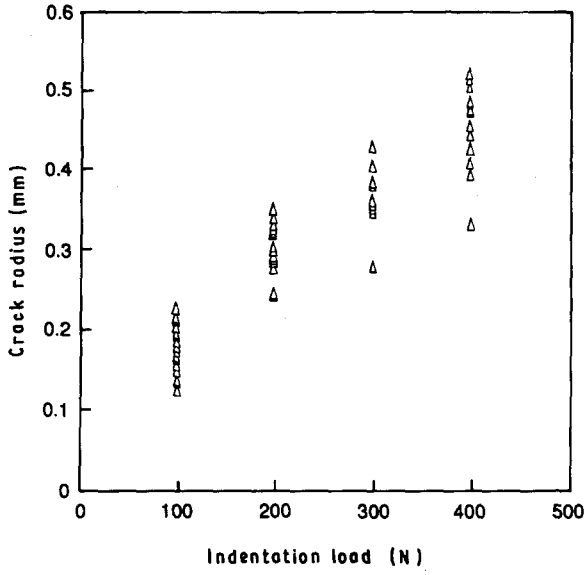

Figure 7 Radius of indentation crack in polished surface of AD-94 alumina as a function of indentation load.

samples and a much better correlation for the Monkman–Grant behaviour.

Fig. 8a and b show the experimental results for the effect of the slots or indentation cracks on the specimen compliance as a function of slot depth or indentation load, respectively. Fig. 8a includes the dependence of the compliance determined experimentally by Bush [19] for slotted circular rods of aluminium subjected to three-point loading adjusted for the loading conditions and sample dimensions for this study and the differences between the Young's moduli of the alumina of this study of $\sim$ 340 GPa and the aluminium of Bush's study taken as 73 GPa. This adjustment to Bush's equation should result in an error of no greater than 20% [20]. In fact, the agreement between the compliances obtained in this study and those based on the modified Bush equation is fairly good. It is of interest to note that a discontinuity exists between the data for zero slot depth and the data point obtained by extrapolation of the experimental data to zero slot depth. It is thought that this discrepancy is the result of "damage" in the form of microcracks introduced during the notching operation, which extend into the matrix phase ahead of the front of the notch.

The data of Fig. 8 indicate that rapid change in compliance with increasing notch depth occurs only after the notch depth-to-diameter ratio has attained a value of about 0.2, which for the diameter of the specimens of this study corresponds to a notch depth of about 1.2 mm. Similarly, an indentation load of about 200 N is required before the compliance becomes significantly affected by the presence of the indentation crack. From Fig. 7, this value of indentation load corresponds to a value of average crack radius of about 0.3 mm.

The measurement of the fracture toughness by the method of Chantikul *et al.* [18], resulted in values of 1.91, 1.93 and 1.94 MPa $m^{1/2}$ at 1225 °C, for samples with indentation cracks introduced at loads of 162,

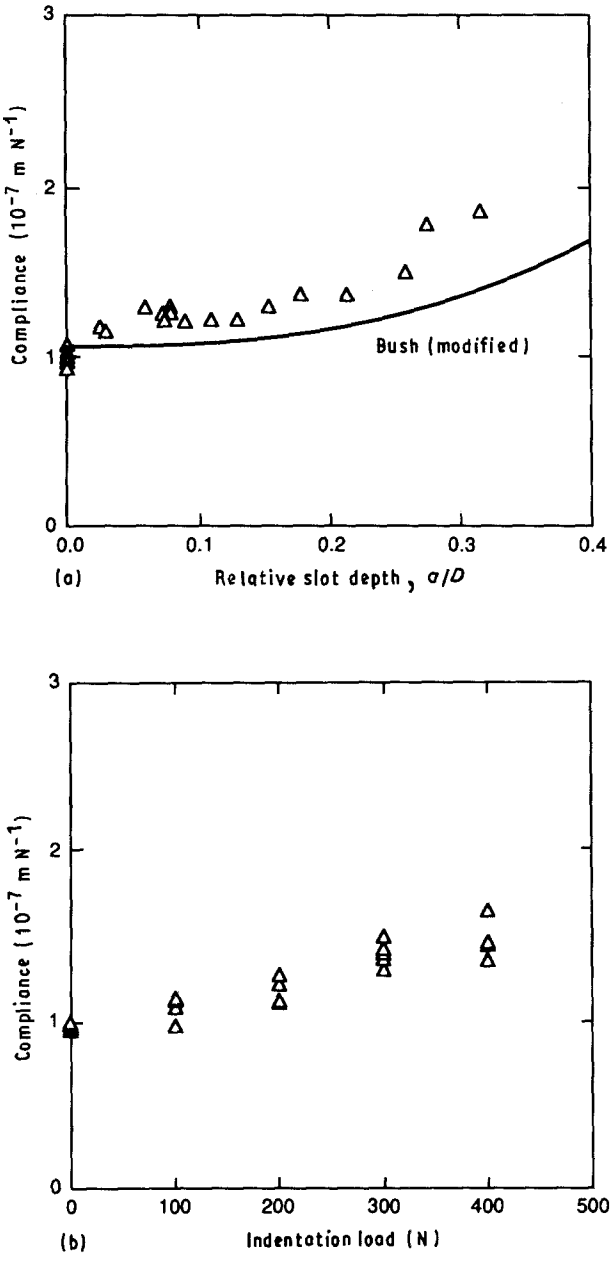

Figure 8 Compliance of AD-94 alumina samples, (a) for slotted samples as function of ratio of slot depth-to-diameter, and (b) for indented samples as a function of indentation load.

250 and 350 N, respectively. These data suggest the existence of a slight *R*-curve effect, i.e. increasing fracture toughness with increasing crack length. However, from the perspective of the experimental uncertainty it will be assumed that the fracture toughness was independent of crack length with a value of 1.93 MPa m$^{1/2}$.

The mean stress required for fracture of the unslotted specimens at 1225 °C under conditions of rapid loading was found to be 60.3 MPa with a standard deviation of 6.2 MPa.

SEM fractography of the surfaces of specimens subjected to creep and fracture under load gave results which were not totally clear-cut. Possibly as the result of the flow of the glassy phase, little or no distinction could be made between the surface features of the fracture surface subjected to sub-critical and fast fracture. For this reason, the size of the crack at the onset of failure could not be equivocally determined. In order to circumvent this problem, a specimen was subjected to creep at a stress of 17.2 MPa for a period of ~ 3 min, and cooled to room temperature prior to fracture. Fig. 9 shows SEM-fractographs near the position of maximum tensile stress and approximately 25, 50 and 75% of the diameter towards the outer surface subjected to maximum compression. These fractographs show distinct differences. Those near the site of maximum tensile stress are typical of fracture surfaces produced at high temperature by intergranular crack propagation. Viscous flow of the glassy phase is also evident. In contrast, those nearer the compressive surface are typical of fracture surfaces which result from transgranular fracture expected for crack propagation near room temperature. These observations indicate that the total fracture surface resulted from fracture at two different temperatures. The high temperature fracture was produced by sub-critical crack propagation. The remainder of the fracture surface resulted from the fast fracture of the specimen at room temperature. Additional observations indicated that this particular crack had propagated approximately 60% along the total diameter of the cross-section during high temperature creep, with the remainder occurring at room temperature. Similar observations on other specimens indicated that crack propagation prior to fracture can extend over a significant fraction of the cross sectional area of the specimen.

For a general analysis of the creep and fracture behaviour data of this study, the general equation for the effect of crack depth on specimen compliance for a circular rod subjected to bending as determined by Bush [19], shown graphically in Fig. 8a after adjustment for the specimen geometry and loading conditions of this study, will be assumed to be valid. The compliance, c, of the specimens of this study, in terms of the ratio of the deflection at the inner loading points to the load as a function of crack-depth can therefore be expressed by

$$c = 105[1 + 5.46(a/D)^{2.5} + 30.2(a/D)^{7}] \times 10^{-9}\ \mathrm{m\,N^{-1}} \quad (1)$$

where a is the crack-depth and D is the specimen diameter.

The Mode I plane-strain stress intensity factor, K_I, can be obtained by noting that the strain energy release rate, G, is related to the change in compliance with increase in crack length by

$$K_I = [GE/(1 - \mu^2)]^{1/2} \quad (2)$$

where E is Young's modulus, μ is Poisson's ratio and

$$G = P^2(\mathrm{d}c/\mathrm{d}a)/2B \quad (3)$$

where P is the specimen load and B is the crack width. For the slot geometry of the samples of this study, the crack width, B, is related to the crack depth, a, and the specimen diameter, D, by

$$B = 2(Da - a^2)^{1/2} \quad (4)$$

The term $\mathrm{d}c/\mathrm{d}a$ can be obtained from Equation 1, and

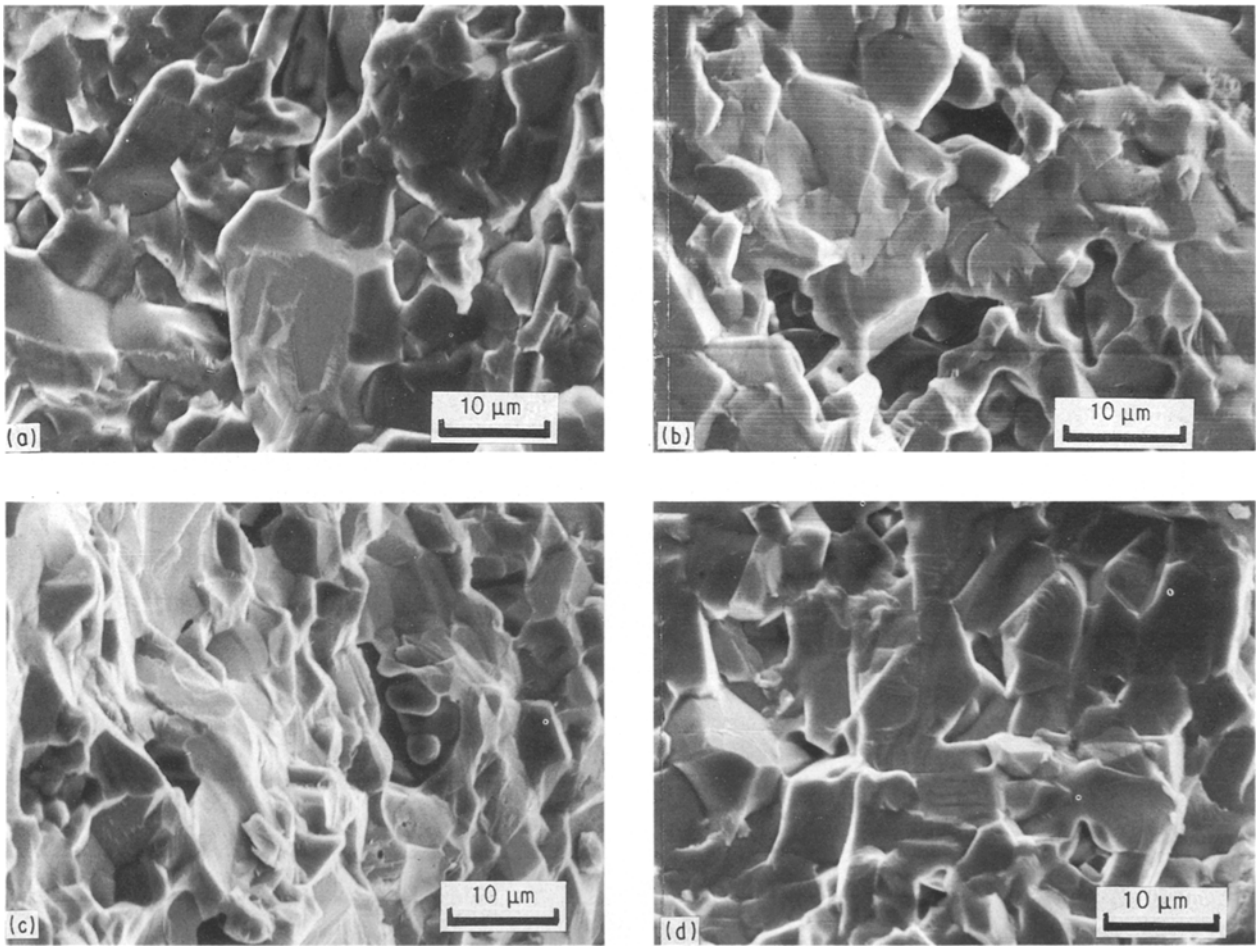

Figure 9 SEM fractographs of AD-94 alumina subjected to interrupted creep deformation at 1225 °C and stress value of 17.2 MPa, followed by fracture at room temperature, (a) at position of maximum tensile stress, and at fractional positions along the diameter equal to approximately (b) 25%, (c) 50% and (d) 75%.

when combined with Equations 2, 3 and 4, the expression for K_I becomes

$$K_I = (10^{-9}\{P^2E[1432(a/D)^{1.5} + 22\,193(a/D)^6]\}/ 4D(1 - \mu^2)(Da - a^2)^{1/2})^{1/2} \quad (5)$$

Because of its complexity, it is more convenient to solve Equation 5 graphically. Fig. 10 shows the K_I value for the specimens of this study as a function of a/D for a range of loads P.

A lower bound for the effect of cracks on creep rate, i.e. crack-enhanced creep, can be obtained by noting that for linear creep the relative increase in creep rate due to the presence of cracks is equal to the corresponding increase in specimen compliance. From Equation 1 this yields

$$\dot{\varepsilon}_c = \dot{\varepsilon}_0[1 + 5.46(a/D)^{2.5} + 30.2(a/D)^7] \quad (6)$$

where $\dot{\varepsilon}_0$ is the creep rate in the absence of cracks. For non-linear creep the relative rate of creep is greater than the relative increase in compliance, as shown by Weertman [12] for a two-dimensional plate with Griffith cracks.

The contribution of crack growth to the creep rate, i.e. elastic creep, can be derived by noting that the outer-fibre strain, ε_m, between the inner loading points in four-point bending from beam-bending theory [21]

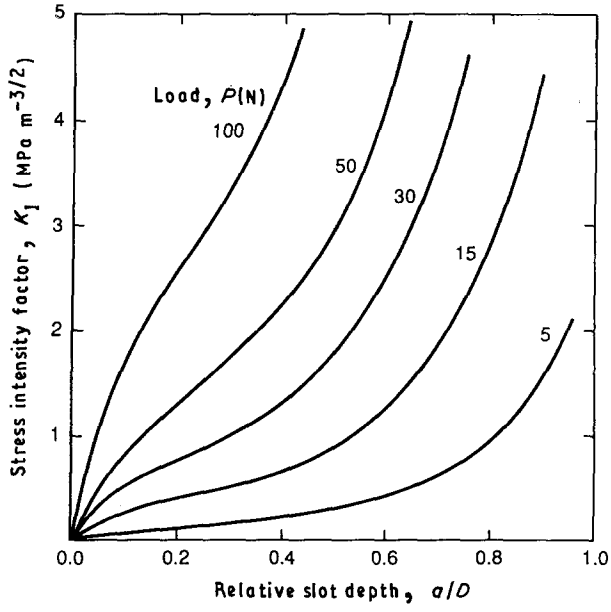

Figure 10 Mode I stress intensity factor for slotted AD-94 alumina samples as a function of ratio of slot depth-to-diameter as calculated from the modified equation of Bush for values of load, P, of 5, 30, 50 and 100 N, which corresponds to values of outer fibre stress of 3.1, 18.4, 30.7 and 61.4 MPa, respectively.

can be derived to be

$$\varepsilon_m = 6PD\{105[1 + 5.46(a/D)^{2.5} + 30.2(a/D)^7]\}/2(3Ld - 4d^2) \quad (7)$$

where L is the distance between the outer loading points, and d is half the difference between the outer and inner loading spans. Differentiating Equation 7 with respect to time results in the elastic creep rate, $\dot{\varepsilon}_{el}$, due to crack growth

$$\dot{\varepsilon}_{el} = 6PD\dot{a}\{105[13.64(a/D)^{1.5} + 211.49(a/D)^6]\}/2(3Ld - 4d^2) \quad (8)$$

where $\dot{a}$ is the rate of crack growth.

For an assessment of the dominant mechanism of creep, it will be assumed that the crack geometry in the creep specimens corresponds to the geometry of the slotted specimens.

The initial flaw size at 1225 °C can be determined from Equation 5 (i.e. Fig. 10), using the mean rapid-fracture stress of 60.3 MPa and the value of fracture toughness of 1.93 MPa $m^{1/2}$, to correspond to a value of a/D of approx. 0.04, which for a specimen diameter of $D = 6.25$ mm, yields a value of crack depth of 0.25 mm. This value of flaw depth is thought to correspond to the dimensions of a pocket of glass as shown in Fig. 2, plus the length of any glassy film which extends along the grain boundary from the pocket of glass. Because of the viscous nature of the glassy phase such a combination of glass pocket and viscous glassy grain boundary acts as an effective crack. Comparison with the data of Fig. 5a for the rate of creep as a function of relative notch depth suggests that a crack depth of 0.25 mm is sufficiently large for crack-enhanced creep to make a significant contribution to the rate of creep even at the onset of the creep deformation.

The crack size at the instance of failure during the creep experiment can be calculated in a similar fashion. For instance, at a stress of 18.6 MPa, the flaw depth at failure with the aid of Fig. 10 can be determined to correspond to a value of the flaw depth-to-diameter ratio of about 0.52, in support of the evidence presented in the scanning electron micrographs of Fig. 9. Again, comparison with the data for the creep rate for the slotted and pre-cracked specimens presented in Figs 5a and 6a suggests that crack-enhanced creep has made a significant contribution to the total creep deformation of the as-received specimens. For the above value of crack depth and specimen diameter the change in specimen compliance calculated from Equation 1 is about 2.54×10^{-7} m N^{-1}, which corresponds to a value of creep strain of about 0.014%. The total value of measured creep strain at failure was of the order of 0.16%. This implies that the contribution of elastic creep by crack growth contributed approximately 9% to the total creep strain. This suggests that for the present experiments elastic creep by crack growth made only a minor contribution to the total creep strain. At the higher stress values, at which failure occurs at smaller crack sizes, the relative contribution of elastic creep will be even lower. This conclusion was supported by the finding that for the slotted specimens for which the creep process was interrupted no significant increase in the specimen compliance could be determined within the accuracy of the measurement. For this reason, the significant increase in the creep rate due to the presence of the slots or indentation cracks must be attributed to the mechanism of crack-enhanced creep. It is anticipated that elastic creep could have made a significant contribution if the creep process had involved multiple crack formation such as observed by the present authors in earlier studies [11, 17], causing much larger changes in specimen compliance. Such multiple crack formation, however, was not observed to have occurred in the specimens of this study.

A few final remarks are in order regarding the correlations between creep rate and time-to-failure. As already noted, an inverse relationship is expected between creep rate and time-to-failure, regardless of whether failure occurred from pre-existing flaws or from creep-constrained flaw nucleation and growth. For this reason a Monkman–Grant type of relationship is to be expected. The same relationship is expected to hold for crack-enhanced creep resulting from the presence of cracks of sufficient size or density that the creep rate is significantly increased over the creep rate in the absence of cracks. These authors wish to refer to this phenomenon as "crack-enhanced creep fracture". Creep deformation by the phenomenon of elastic creep by crack growth is also expected to exhibit a Monkman–Grant type of behaviour as the time-to-failure is an inverse function of the rate of crack growth, whereas the corresponding rate of creep is directly proportional to the rate of crack growth. Conventional creep (in the absence of crack growth), crack-enhanced creep and elastic creep by crack growth all are expected to exhibit better correlations between creep rate and time-to-failure than between stress and creep rate or time-to-failure, as demonstrated by the three sets of data of this study.

Acknowledgement

This study was conducted as part of a research programme supported by the Army Research Office under Contract no. DAAL03-88-K-0073.

References

1. S. M. JOHNSON, B. J. DALGLEISH and A. G. EVANS, *J. Amer. Ceram. Soc.* **67** (1984) 759.
2. B. J. DALGLEISH and A. G. EVANS, *ibid.* **68** (1985) 44.
3. B. J. DALGLEISH, E. B. SLAMOVICH and A. G. EVANS, *ibid.* **68** (1985) 575.
4. D. R. CLARKE, *J. Mater. Sci.* **20** (1985) 1321.
5. S. M. WIEDERHORN, B. J. HOCKEY, R. F. KRAUSE Jr and K. JAKUS, *ibid.* **21** (1986) 810.
6. G. D. QUINN, *ibid.* **22** (1987) 2309.
7. F. F. LANGE, B. I. DAVIS and D. R. CLARKE, *ibid.* **15** (1980) 601.
8. H. S. Y. HSICH, *ibid.* **15** (1980) 1194.
9. J. R. DRYDEN, D. KUCEROVSKY, D. S. WILKINSON and D. F. WATT, *Acta Metall.* **37** (1989) 2007.
10. F. C. MONKMAN and N. J. GRANT, *Proc. ASTM* **56** (1956) 593.
11. D. P. H. HASSELMAN, A. VENKATESWARAN and K. Y. DONALDSON, *J. Mater. Sci.* **24** (1989) 565.

12. J. WEERTMAN, *Trans. Amer. Soc. Met.* **62** (1969) 502.
13. D. P. H. HASSELMAN and A. VENKATESWARAN, *J. Mater. Sci.* **18** (1983) 161.
14. *Idem.*, in "Deformation of Ceramic Materials II", edited by R. E. Tressler and R. C. Bradt (Plenum Press, New York, 1984) pp. 525–45.
15. A. VENKATESWARAN and D. P. H. HASSELMAN, *J. Mater. Sci.* **16** (1981) 1627.
16. S. SURESH and J. R. BROCKENBROUGH, *Acta Metall. Mater.* **38** (1990) 55.
17. A. VENKATESWARAN, K. Y. DONALDSON and D. P. H. HASSELMAN, *J. Amer. Ceram. Soc.* **71** (1988) 565.
18. P. CHANTIKUL, G. R. ANSTIS, B. R. LAWN and D. B. MARSHALL, *ibid.* **64** (1981) 539.
19. A. J. BUSH, *Exp. Mech.* **16** (1976) 249.
20. W. C. SMITH, private communication (July, 1989).
21. E. P. POPOV, in "Mechanics of Materials", 2nd Edn (Prentice-Hall, Englewood Cliffs, NJ, 1976) p. 580.

Received 24 April
and accepted 2 August 1991